

# Constraints on the mean free path of ionising photons at $z \sim 6$ using limits on individual free paths

SARAH E. I. BOSMAN<sup>1</sup>

<sup>1</sup>*Max-Planck-Institut für Astronomie, Königstuhl 17, D-69117 Heidelberg, Germany*

## ABSTRACT

The recent measurement of an ionising mean free path  $\lambda_{\text{mfp}} < 1$  pMpc at  $z = 6$  challenges our understanding of the small-scale structure of the intergalactic medium (IGM) at the end of reionisation. We introduce a new method to constrain  $\lambda_{\text{mfp}}$  at  $z = 6$  by using lower limits on the individual free paths of ionisation around quasars. Lyman-limit absorbers with a density sufficient to halt ionising photons produce strong absorption in the 6 lowest-energy Lyman transitions, in the absence of which a robust lower limit can be placed on the individual free path. Applying this method to a set of 26 quasars at  $5.5 < z < 6.5$ , we find that 80% of bright quasars ( $M_{1450} < -26.5$ ) require individual free paths larger than 2 pMpc. We model the relation between opacity  $\kappa$  and photo-ionisation rate  $\Gamma$  via the parameter  $\xi$  such that  $\kappa \propto \Gamma^{-\xi}$ , and pose joint limits on  $\lambda_{\text{mfp}}$  and  $\xi$ . For the nominal value of  $\xi = 2/3$ , we constrain  $\lambda_{\text{mfp}} > 0.31$  (0.18) pMpc at  $2\sigma$  ( $3\sigma$ ): a much tighter lower bound than obtained through traditional stacking methods. Our constraints get significantly stronger for lower values of  $\xi$ . New constraints on  $\lambda_{\text{mfp}}$  and  $\xi$  are crucial to our understanding of the reionisation-era IGM.

*Keywords:* Lyman limit systems(981) — Quasar absorption line spectroscopy(1317) — Intergalactic medium(813) — Reionization(1383)

## 1. INTRODUCTION

The reionisation of hydrogen in the inter-galactic medium (IGM) is driven by ionising radiation emitted by the first stars. The unfolding of reionisation is therefore tightly linked to the evolving ionising emissivity of the first galaxies, but is also regulated by the average distance that ionising photons can travel through the IGM - the ionising mean free path  $\lambda_{\text{mfp}}$ .

A fast increase in  $\lambda_{\text{mfp}}$  is an expected marker of the end of the reionisation process, indicating that the ionising background becomes percolated (Gnedin 2000; Gnedin & Fan 2006; D’Aloisio et al. 2018; Kulkarni et al. 2019; Keating et al. 2020b; Nasir & D’Aloisio 2020). Recently, Becker et al. (2021) reported the measurement of a very short  $\lambda_{\text{mfp}} = 0.75_{-0.45}^{+0.65}$  pMpc at  $z = 6.0$  and its increase by a factor of 12 by  $z = 5.1$ . Such a fast evolution would constitute a smoking gun of reionisation’s end, adding to mounting evidence that the process completes at  $z \lesssim 6.0$  (e.g. Becker et al. 2015, 2018; Bosman et al. 2018, 2021b; Boera et al. 2019; Jung et al.

2020; Kashino et al. 2020; Morales et al. 2021, etc). A mean free path of  $< 1$  pMpc at  $z = 6$  requires the ionising emissivity of early galaxies to be significantly higher than observed in  $z \leq 3$  galaxies (Cain et al. 2021; Davies et al. 2021). Constraints on the mean free path at  $z \gtrsim 6$ , at the end stages of reionisation, are thus a crucial element for models of the high- $z$  IGM.

The ionising mean free path has been measured with methods falling broadly in three categories. First, the mean free path and the photo-ionisation rate ( $\Gamma$ ) of the ultra-violet background (UVB) can be inferred in a model-dependent manner from measurements of the mean Lyman- $\alpha$  optical depth, provided the global emissivity of sources is known (Miralda-Escude & Ostriker 1990; Meiksin & Madau 1993; Haardt & Madau 1996; Faucher-Giguère et al. 2008). At  $z > 5.5$ , the origin of UVB fluctuations is currently still debated and the global emissivity is unknown, therefore constraints are likely to be more model-dependent than at  $z < 5$  (Davies & Furlanetto 2016; D’Aloisio et al. 2018; Nasir & D’Aloisio 2020). A second category of methods consists in measuring the decline of the average transmitted flux of quasars at wavelengths shorter than the Lyman limit ( $\lambda = 911.76\text{\AA}$ ). The mean free path is defined as the distance over which the ionising flux has declined

by a fraction  $1/e$ , corresponding to an opacity  $\tau = 1$ . The flux decrease beyond the Lyman limit is therefore a direct measurement of  $\lambda_{\text{mfp}}$  (Prochaska et al. 2009; Fumagalli et al. 2013; O’Meara et al. 2013; Worseck et al. 2014; Becker et al. 2021).

In this paper, we introduce a new method which most closely resembles the third approach: constraining the propagation distance of ionising radiation from individual sources (the individual free paths) via the distributions of absorbers which limit the propagation of radiation (Songaila & Cowie 2010; Rudie et al. 2013; Romano et al. 2019). In practice, the propagation of ionising photons is often halted by encounters with discrete Lyman-limit systems (LLS) with  $\log N_{\text{HI}} \gtrsim 17.2 \text{ cm}^{-2}$ . The distance from a quasar to the nearest LLS therefore poses a stringent lower limit on the individual free path around the object. Whereas Songaila & Cowie (2010) and Romano et al. (2019) identify a quasar’s nearest LLS via absorption at the Lyman limit, we instead use the fact that an LLS will saturate all 6 of the lowest-energy Lyman-series transitions (Ly- $\alpha$  to Ly- $\zeta$ ). Our method therefore has the advantage of requiring no transmission at the Lyman limit in order to pose constraints. Indeed, the overlapping Lyman-series transmission at the Lyman limit is predicted to be exceedingly weak (Becker et al. 2021).

We explain our method in more detail in Section 2. We conduct a demonstration of the measurement on a sample of 26 quasars at  $5.5 \lesssim z \lesssim 6.5$  and we present the individual free path constraints in Section 3. The resulting limits on individual free paths place the potential LLS in regions where the photo-ionisation rate is dominated by the quasars rather than the UVB. To account for this effect, we employ the general framework developed by Becker et al. (2021) and give details in Section 4. The mean free path away from the quasar’s influence then depends on  $\Gamma$  via a free parameter  $\xi$ . In Section 5, we present joint constraints on  $\lambda_{\text{mfp}}$  and  $\xi$  and compare with previous measurements. We conclude in Section 6.

Throughout the paper we assume a Planck Collaboration et al. (2020) cosmology with  $H_0 = 67.74$ ,  $\Omega_m = 0.3089$ . Wavelengths always refer to the rest-frame unless explicitly stated. Comoving and proper distances are always labelled explicitly (e.g. cMpc).  $M_{1450}$  corresponds to the absolute magnitude at  $\lambda = 1450\text{\AA}$ .

## 2. MEASURING INDIVIDUAL FREE PATHS WITH THE LYMAN SERIES

The optical depth of the IGM to ionising radiation at a distance  $r$  from a source of radiation is given by  $\tau_{912} = -\ln(F(r)/F_0)$  in the rest frame of the absorbing

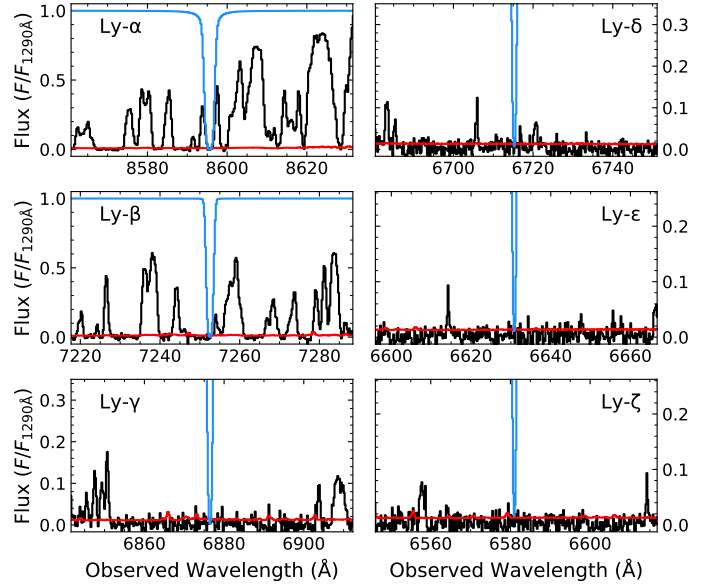


**Figure 1.** Example of the highest- $z$  possible LLS location in quasar J1319+0950. Note how saturated Ly- $\alpha$  absorbers do occur closer to the quasar (top left panel), but none of them are also opaque in Ly- $\beta$  and Ly- $\gamma$  (middle left and bottom left panels). The simulated absorbers have been forward-modelled to the resolution and pixel size of X-Shooter, assuming  $b = 15 \text{ km s}^{-1}$ . Note that the scale of the  $y$ -axis changes between figures.

gas, where  $F_0$  is the ionising flux emitted by the source and  $F(r)$  is the transmitted flux at distance  $r$ . Additionally,  $\tau_{912} = \int_{r'=0}^r \kappa(r') dr'$ , where  $\kappa(r) = d\tau(r)/dr$ . In a uniform medium, the definition of  $\lambda_{\text{mfp}}$  as the distance such that  $\tau = 1$  therefore leads to  $\lambda_{\text{mfp}} = 1/\kappa$ .

In practice, the propagation of ionising radiation is halted by stochastic absorbers which individually have  $\tau \gtrsim 1$ , corresponding to a column density of neutral gas  $\log N_{\text{HI}}/\text{cm}^{-2} \gtrsim 17.2$ . In addition to suppressing ionising radiation at  $\lambda < 912\text{\AA}$ , such absorbers will necessarily produce strong absorption in the lowest-energy Lyman transitions, i.e. Ly- $\alpha$  1215.67 $\text{\AA}$ , Ly- $\beta$  1025.72 $\text{\AA}$ , Ly- $\gamma$  972.53 $\text{\AA}$ , Ly- $\delta$  949.74 $\text{\AA}$ , Ly- $\epsilon$  937.80 $\text{\AA}$  and Ly- $\zeta$  930.74 $\text{\AA}$ , to list the first 6). For example, a neutral hydrogen absorber capable of saturating Ly- $\alpha$  but not Ly- $\beta$  absorption can have a column density no higher than  $\log N_{\text{HI}}/\text{cm}^{-2} \simeq 15.5$ . As seen in the lower-redshift Ly- $\alpha$  forest, even dozens of such absorbers do not result in significant absorption at the Lyman limit (e.g. Songaila & Cowie 2010, but see discussion of the contribution of absorbers with  $N_{\text{HI}}/\text{cm}^{-2} \gtrsim 16.5$  in Sec. 5.1). For a LLS, absorption in the first 6 Lyman transitions (at least) will occur in the non-linear regime of the curve of growth, resulting in flat central absorption troughs.

We use this property to find the nearest location from a quasar at which all 6 transitions are strongly absorbed, directly corresponding to the *nearest location at which a LLS could be located*. Straightforwardly, the individual free path of ionisation around the source can be no shorter than this limit. Overlap with foreground Ly- $\alpha$  absorption will lead, on average, to the limit being an under-estimate of the true individual free path; but it cannot be an over-estimate.

The width of absorption troughs in the Lyman-series transitions depends on the Doppler parameter  $b$ . In the  $z \sim 6$  IGM, thermal broadening alone results in  $b \geq 10$  km s $^{-1}$  (Gaikwad et al. 2020). However, inside the proximity zones where our limits on the individual free paths are located, photo-ionisation heating results in  $b > 20$  km s $^{-1}$  for  $> 80\%$  of hydrogen absorbers (Bolton et al. 2010, 2012). We therefore opt for a nominal choice of  $b = 15$  km s $^{-1}$  (see Sec. 5.1 for further discussion of this choice). We generate Voigt profiles and forward-model them to the spectral resolution and pixel scales of the X-Shooter instrument, of 34 km s $^{-1}$  and 10 km s $^{-1}$  respectively (Vernet et al. 2011). Spectroscopy of quasars with X-Shooter often achieves resolution superior to the nominal, closer to 28 km s $^{-1}$  (see e.g. Bosman et al. 2017). We find that even at nominal resolution, the first 3 Lyman series transitions are absorbed to less than 2% transmission per pixel over the central 3 pixels of the absorption troughs, and the next three transitions to less than 5% transmission per pixel. We therefore select a criterion for candidate LLS locations of non-detections at the  $3\sigma$  level over 3 pixels, which determines the sensitivity level required of our observations (roughly SNR  $\geq 10$  per pixel). We neglect performing a reconstruction of the underlying continuum of the quasars, since obtaining accurate predictions (even within 30%) down to 930Å is highly impractical and limited by the availability of low- $z$  training samples (Bosman et al. 2021a).

### 3. OBSERVATIONS

We use a sample of 26 quasars at  $5.5 \lesssim z \lesssim 6.5$  observed with X-Shooter to a depth of SNR  $\geq 10$  per 10 km s $^{-1}$  pixel (Table 1). All spectra were presented and used in the analysis of Bosman et al. (2021b), where more details can be found regarding the data reduction. The systemic redshifts of the quasars are obtained either from detections of the sub-mm emission lines of their host galaxies, or via the redshift of occurrence of the first IGM hydrogen absorber. The latter technique has an accuracy of  $\Delta v = 180 \pm 180$  km s $^{-1}$  compared to the former (Becker et al. 2021), corresponding to an uncertainty in the distance to the first candidate LLS location of  $\Delta r = 0.2$  pMpc. We neglect this uncertainty.

Quasar name	$z_{\text{qso}}$	$M_{1450}$	max $z_{\text{LLS}}$	min $\lambda_{\text{ifp}}$ /pMpc	refs.
J036+03	6.5405	-27.33	6.4847	2.850	(1,2)
J011+09	6.4695	-25.95	6.4227*	2.446	(3,4)
J159-02	6.3860	-26.80	6.3584	1.477	(5,6)
J0100+2802	6.3269	-29.14	6.1955	7.264	(7,2)
J025-33	6.318	-27.81	6.2454*	4.001	(8,9)
J1030+0524	6.309	-26.99	6.2425	3.674	(10,11)
J0330-4025	6.239	-26.42	6.2309	0.452	(12,13)
J308-21	6.2355	-26.35	6.2350	0.024	(5,2)
J2318-3029	6.1456	-26.16	6.1334	0.706	(14,2)
J1319+0950	6.1347	-27.05	6.0711	3.730	(15,2)
J1509-1749	6.1225	-27.14	6.1092	0.778	(16,17)
J2100-1715	6.0807	-25.55	6.0806	0.001	(18,2)
J1207+0630	6.0366	-26.63	6.0051	1.902	(19,17)
J1306+0356	6.033	-26.81	5.9190*	6.101	(10,2)
J340-18	5.999	-26.42	5.9331	0.007	(20,9)
J0148+0600	5.998	-27.39	5.9437	3.338	(19,9)
J0818+1722	5.997	-27.52	5.9532	2.706	(21,9)
J0046-2837	6.021	-25.42	6.0201	0.051	(22,23)
J056-16	5.9676	-26.72	5.9551	0.772	(5,4)
J004+17	5.8166	-26.01	5.8164	0.012	(5,4)
J0836+0054	5.804	-27.75	5.4682*	22.888	(10,6)
J0927+2001	5.7722	-26.76	5.7036*	4.586	(21,23)
J215-16	5.7321	-27.54	5.7314	0.043	(24,24)
J1335-0328	5.693	-27.76	5.5938*	6.853	(25,9)
J0108+0711	5.577	-27.19	5.4531*	8.975	(25,9)
J2207-0416	5.529	-27.70	5.4699	4.326	(26,9)

**Table 1.** The quasars used in this work, with their physical and measured properties. Quasar redshifts with 5 significant figures indicate the redshifts were obtained from sub-mm emission lines. Stars next to  $z_{\text{LLS}}$  indicate that detection of significant Lyman continuum transmission refined the constraints (7/26 quasars). References correspond to (Discovery, Redshift): (1) Venemans et al. 2015; (2) Venemans et al. 2020; (3) Mazzucchelli et al. 2017; (4) Eilers et al. 2021b; (5) Bañados et al. 2016; (6) Bosman et al. 2021b; (7) Wu et al. 2015; (8) Carnall et al. 2015; (9) Becker et al. 2019; (10) Fan et al. 2001; (11) Jiang et al. 2007; (12) Reed et al. 2017; (13) Eilers et al. 2020; (14) Farina et al. 2019; (15) Mortlock et al. 2009; (16) Willott et al. 2007; (17) Decarli et al. 2018; (18) Willott et al. 2010; (19) Jiang et al. 2015; (20) Bañados et al. 2015; (21) Fan et al. 2006; (22) Venemans et al. 2018; (23) Schindler et al. 2020; (24) Morganson et al. 2012; (25) Yang et al. 2017; (26) Wang et al. 2016

Table 1 lists the locations of the nearest possible LLS from each quasar. Figure 1 shows an example of the first possible location of a LLS in quasar J1319+0950. Similar figures for all the quasars in our sample can be found in Appendix A. For 7/26 quasars, the constraints can

be improved based on the occurrence of strong spikes of Lyman-continuum transmission at a lower redshift than our method alone. We conservatively define strong Lyman-continuum transmission as broad emission features detected at  $> 1\sigma$  over 6 consecutive pixels, and at  $> 4\sigma$  overall. When Lyman continuum transmission is detected, we start the search for a LLS at  $z \leq z_{\text{spike}}$  rather than  $z \leq z_{\text{qso}}$ , resulting in a lower  $\max(z_{\text{LLS}})$ . The quasars for which Lyman continuum transmission provided an additional constraint are indicated by stars in Table 1. Figures showing the corresponding Lyman-continuum spikes for those 7 quasars can be found in Appendix B.

Figure 2 shows the resulting lower limits on individual free paths as a function of the quasar intrinsic magnitude  $M_{1450}$ . All of our lower limits on the individual free paths, except one, correspond to distances within the quasars' proximity zones with  $r < R_{\text{eq}}$  (see Section 4). The sightline to quasar J0836+0054 is the sole exception. The lack of LLS absorption extends to a distance of 24.0 pMpc in front of this object, 40% longer than the quasar's expected influence given its  $M_{1450}$ . This suggests that J0836+0054, in addition to being highly luminous, happens to reside in a large-scale under-density (see also Becker et al. 2021). Three quasars in our sample were targeted as potential 'young' quasars with short Ly- $\alpha$  proximity zones (Eilers et al. 2020). Two of them belong the lowest third of quasar magnitudes in our sample, among which one young quasar poses the weakest constraint (J2100–1715, tied with the non-young quasar J0046–2837) and one poses the tightest constraint on the individual free path (J011+09). We therefore find no qualitative difference between these quasars with the shortest proximity zones from the general population in terms of possible proximity to a LLS. We will return to this point in Section 5.1.

The trend of longer individual free paths with quasar brightness is a general theoretical expectation. Brighter quasars produce higher  $\Gamma(r)$  in their environments, efficiently photo-ionising hydrogen and leading to longer individual free paths as well as fewer hydrogen absorbers in general. Our model must therefore account for the quasars' ionising effects when computing the permitted  $\lambda_{\text{mfp}}$  in the IGM away from bright sources. We do not observe a trend in individual free path limits with redshift across our sample.

#### 4. MODEL

In order to relate our limits on individual free paths around quasars to  $\lambda_{\text{mfp}}$  in the general IGM, we use the theoretically-motivated scaling of opacity with ionisa-

tion rate parametrised by a scaling parameter  $\xi$ :

$$\kappa(\Gamma) = \kappa_{\text{bg}} \left( \frac{\Gamma}{\Gamma_{\text{bg}}} \right)^{-\xi}, \quad (1)$$

where  $\Gamma_{\text{bg}}$  is the ionisation rate in the IGM at  $z = 6$ , which we set to  $\Gamma_{\text{bg}} = 3 \times 10^{-13} \text{ s}^{-1}$  as measured by Becker et al. (2021) (see Section 5.1). In a uniform and static medium,  $\kappa_{\text{bg}} = 1\lambda_{\text{mfp}}$ . We adopt the general framework used by Becker et al. (2021) to build a model which predicts the mean free path around a quasar of magnitude  $M_{1450}$  as a function of the background  $\lambda_{\text{mfp}}$  and the scaling parameter  $\xi$ .

The quasar sources a photo-ionisation rate which falls off quadratically with proper distance in an optically-thin medium:

$$\frac{\Gamma_{\text{qso}}(r)}{\Gamma_{\text{bg}}} = \left( \frac{R_{\text{eq}}}{r} \right)^2, \quad (2)$$

where  $R_{\text{eq}}$  is the equilibrium distance at which  $\Gamma_{\text{qso}}(R_{\text{eq}}) = \Gamma_{\text{bg}}$  (Calverley et al. 2011). To obtain  $R_{\text{eq}}$ , we use the scaling relation from Davies et al. (2020):

$$R_{\text{eq}} = 11.3 \left( \frac{\Gamma_{\text{bg}}}{2.5 \times 10^{-13} \text{ s}^{-1}} \right)^{0.5} \times \left( \frac{\dot{N}_{\text{ion}}}{1.73 \times 10^{57} \text{ s}^{-1}} \right)^{-0.5} \text{ pMpc}, \quad (3)$$

where  $\dot{N}_{\text{ion}}$  is the number of ionising photons emitted by the quasar per second. Finally,  $\dot{N}_{\text{ion}}$  is obtained by extrapolating the spectral energy distribution of the quasar from  $M_{1450}$  following a double power-law with  $L(\nu) \propto \nu^{-\alpha_{\text{UV}}}$  at  $912 < \lambda < 1450 \text{ \AA}$ , and  $L(\nu) \propto \nu^{-\alpha_{\text{ion}}}$  at  $\lambda < 912 \text{ \AA}$ . We use  $\alpha_{\text{UV}} = 0.6$  and  $\alpha_{\text{ion}} = 1.5$  following Lusso et al. (2015) (see Section 5.1).

To account for the absorption by residual neutral gas inside proximity zones, we solve equations (1) and (2) self-consistently by computing the radial profiles over small, optically-thin steps in radius  $\Delta r$  (see Davies & Furlanetto 2014; Davies 2020; Becker et al. 2021):

$$\tau(r+\Delta r) = \tau(r) + \frac{1}{\lambda_{\text{mfp}}} \int_{r'=r}^{r'=r+\Delta r} \left( 1 + \frac{\Gamma_{\text{qso}}(r')}{\Gamma_{\text{bg}}} \right)^{-\xi} dr'; \quad (4)$$

$$\Gamma_{\text{qso}}(r + \Delta r) = e^{-\tau(r+\Delta r)} \Gamma_{\text{bg}} \left( \frac{R_{\text{eq}}}{r + \Delta r} \right)^2. \quad (5)$$

We finally obtain  $\lambda_{\text{mfp}}$  via

$$1 = \int_{r=0}^{r=\lambda_{\text{mfp}}} \kappa(r) dr. \quad (6)$$

We refer the interested reader to Becker et al. (2021) for more details of the framework.



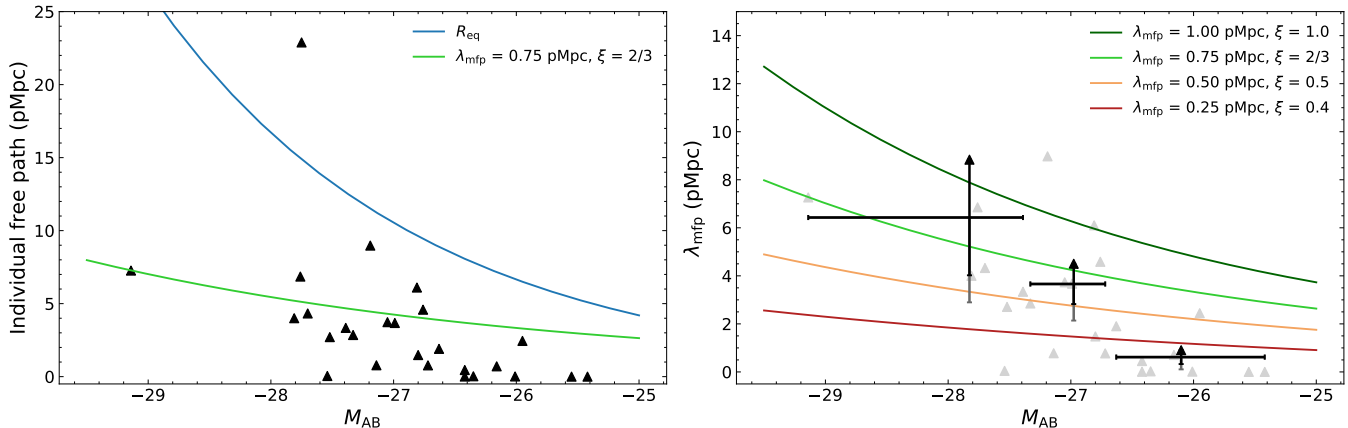


**Figure 2.** Left: Limits on individual free paths as a function of  $M_{AB}$  (black triangles) and expected proximity zone radius  $R_{eq}$  (blue curve). Right: Limits on the mean free path and model curves, color-coded by degree of disagreement with the data (increasing green to red). The black bars represent the means of the individual free path limits, with the lower error bars encompassing 84% (black) and 95% (grey) of the bootstrap-resampled averages.

The resulting curves of  $\lambda_{mfp}$  as a function of  $M_{1450}$  and  $\xi$  are shown in Figure 2. In general, models with high  $\xi \geq 2/3$  and  $\lambda_{mfp} \geq 0.75$  pMpc are consistent with  $> 50\%$  of individual free path limits at all magnitudes, which suggests that they are permitted by the observations. Conversely, models with a short  $\lambda_{mfp}$  and small  $\xi$  increasingly fail to account for the large fraction ( $> 80\%$ ) of bright  $M_{1450} < -26.5$  quasars which do not allow for short individual free paths.

To quantify the level of tension between our models and the individual free path constraints, we first divide the sample into 3 magnitude bins containing roughly the same number of objects (9, 9 and 8 objects from the faintest bin to the brightest) as shown in Figure 2. The mean free path is equal to the mean of individual free paths, which can be *no lower than* the mean of our lower limits on individual free paths. We therefore compute the mean of the individual free path limits in each magnitude bin. We calculate the uncertainty on these “minimum  $\lambda_{mfp}$  limits” by bootstrap-resampling the objects 40000 times within each bin. The lower limits which encompass 84% and 95% of the re-sampled distribution correspond to the  $1\sigma$  and  $2\sigma$  lower bounds on  $\lambda_{mfp}$ , respectively. The probability of a given  $\lambda_{mfp}$  can then be obtained by integrating the distribution of re-sampled means from zero to  $\lambda_{mfp}$ , i.e. over the range of real  $\lambda_{mfp}$  values which are compatible with the model’s prediction. Formally, this procedure amounts to calculating the probability of the model given the observations. Note that we cannot rule in favour of particular values of the parameters, but only establish which set of  $\{\lambda_{mfp}, \xi\}$  are in tension with the limits on individual free paths.

## 5. RESULTS

Figure 3 shows the level of tension between models and the individual free path constraints over parameter ranges  $\lambda_{mfp} = [0.1, 2.0]$  and  $\xi = [0.1, 2.0]$ . The short  $\lambda_{mfp}$  value measured at  $z = 6$  by Becker et al. (2021), of  $\lambda_{mfp} = 0.75^{+0.65}_{-0.45}$ , is permitted by our observations if  $\xi = 2/3$  as assumed nominally by the authors. The value of  $\xi$  is tied to the physical properties of the LLS responsible for setting  $\lambda_{mfp}$ ;  $\xi = 2/3$  is a theoretical expectation if their density profiles are isothermal (Furlanetto & Oh 2005; McQuinn et al. 2011). For  $\xi = 2/3$ , our observations pose constraints on the mean free path of  $\lambda_{mfp} > 0.53$  (0.31, 0.18) pMpc at  $1\sigma$  ( $2\sigma$ ,  $3\sigma$ ). Our  $2\sigma$  lower limits on  $\lambda_{mfp}$  are more constraining than those obtained from stacking transmission at the Lyman-limit ( $\lambda_{mfp} > 0.1$  pMpc at  $2\sigma$ ; Becker et al. 2021).

Lower or higher values of the scaling parameter  $\xi$  have been suggested in the literature. Based on hydrodynamical simulations of dense self-shielded absorbers in the IGM, McQuinn et al. (2011) and D’Aloisio et al. (2020) obtain values of  $\xi = 0.75$  and  $\xi = 0.33$ , respectively. Under the latter assumption for  $\xi$ , our observations pose tight lower limits of  $\lambda_{mfp} > 1.46$  (1.00, 0.68) pMpc at  $1\sigma$  ( $2\sigma$ ,  $3\sigma$ ). These limits are again in agreement with the measurements of Becker et al. (2021) under the same assumption, but our lower limits are more stringent (Fig. 3). For  $\xi \geq 0.75$ , our method quickly becomes non-constraining because the expected  $\lambda_{mfp}$  around quasars becomes increasingly disconnected from the background  $\lambda_{mfp}$ .

Conversely, individual free paths can provide lower limits on  $\xi$  given an assumption for  $\lambda_{mfp}$ . The reionisation models of D’Aloisio et al. (2020) and Keating et al. (2020a) predict  $2 \lesssim \lambda_{mfp} \lesssim 4$  pMpc at  $z = 6$ . Nu-

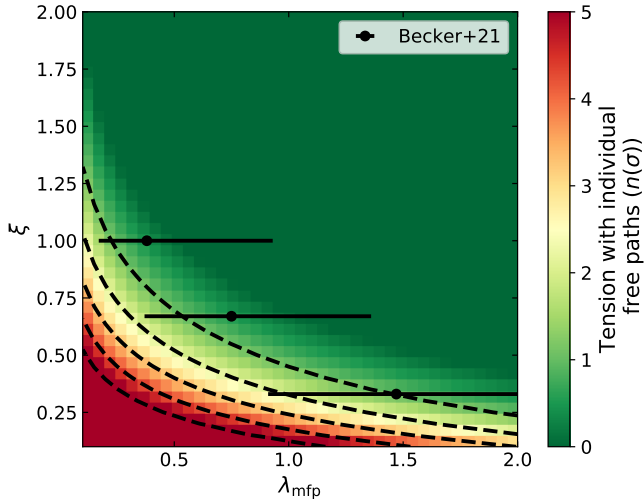


**Figure 3.** Posterior distribution of  $\xi$  and  $\lambda_{\text{mfp}}$  at  $z \sim 6$ . The green-yellow-red color indicates the level of tension between the corresponding  $\xi - \lambda_{\text{mfp}}$  model and the limits on individual free paths around quasars. The dashed curves delineate the bottom-left corner of parameter space, which is ruled out at 1, 2, 3, 4, 5 $\sigma$  (curves in order of decreasing corner area). The  $\lambda_{\text{mfp}}$  measurements from Becker et al. (2021) are shown for the authors’ three different assumptions on  $\xi$  (0.33, 2/3, 1.0).

merical simulations of the mean free path during reionisation have generally predicted a  $\lambda_{\text{mfp}}$  in the range of  $1 \lesssim \lambda_{\text{mfp}} \lesssim 6$  pMpc ( $\lambda_{\text{mfp}} \sim 6$  pMpc, Alvarez & Abel 2012;  $\lambda_{\text{mfp}} \sim 1.2$  pMpc, Emberson et al. 2013;  $4 < \lambda_{\text{mfp}} < 10$  pMpc, Rahmati et al. 2013). The majority of these models are in tension with the nominal measurement of Becker et al. (2021); one way to ease the tension may be to invoke lower values of  $\xi$  (Fig. 3). Our method becomes more constraining in the low- $\xi$  regime. Assuming a value of  $\lambda_{\text{mfp}} = 2$  pMpc, our observations constrain a lower limit for  $\xi > 0.24$  (0.16, 0.10) at 1 $\sigma$  (2 $\sigma$ , 3 $\sigma$ ). Using joint constraints on  $\lambda_{\text{mfp}}$  from stacking at the Lyman limit and individual free paths is therefore a promising way to study the physical state of the  $z \sim 6$  IGM.

### 5.1. Caveats

We discuss the impact of assumptions made in the analysis on our results, including the width of absorbers, uncertainties in model parameters, and the limitations of our formalism.

*Width of absorbers:* Absorbers with Doppler broadening  $b \lesssim 12$  km s $^{-1}$  would not saturate the first 6 Lyman transitions to the thresholds we have used in our measurements due to the relatively low resolution of X-Shooter. The temperature of the IGM at  $z = 5.8$  is  $T \sim 12,000$  K (Gaikwad et al. 2020), corresponding to a floor of purely thermal broadening of  $b \simeq 10$  km s $^{-1}$

(but note that LLS are denser than the low-density IGM and thus potentially hotter). In a spectroscopically resolved analysis of hydrogen absorbers near quasars at  $z \sim 6$ , Bolton et al. (2010, 2012) instead found  $b > 20$  km s $^{-1}$  for over 80% of Ly- $\alpha$  absorbers; the extra broadening is attributed to heating of the gas by the quasar to higher temperatures than the general IGM due to the ionisation of helium ( $T \sim 16000$ K) and potentially additional kinematic broadening. Still, cold gas may conceivably be found inside quasar proximity zones, especially if the quasar phase started relatively recently and the helium-reionisation front has not yet reached the gas. To overcome this limitation, higher-resolution spectroscopy is necessary in order to resolve the widths of individual absorbers and check whether saturated absorption lines possess opaque troughs as expected. Unfortunately, samples of high-resolution  $z > 5.5$  quasar spectra do not yet exist in comparable numbers as the X-Shooter spectra used in this work.

The assumed width of absorbers also relates to a caveat concerning the column densities of hydrogen absorbers which dominate the mean free path. Absorbers with  $\log N_{\text{HI}}/\text{cm}^{-2} \leq 17.0$  have been argued to contribute significantly to limiting the propagation of ionising photons (e.g. Prochaska et al. 2010; Haardt & Madau 2012; Rahmati & Schaye 2018) rather than  $\lambda_{\text{mfp}}$  being limited by the first encounter with a LLS. However, the same criteria of absorption in Ly- $\alpha$  through Ly- $\zeta$  employed in this work would be satisfied by an absorber with  $\log N_{\text{HI}}/\text{cm}^{-2} \geq 16.8$  for  $b = 20$  km s $^{-1}$ , and  $\log N_{\text{HI}}/\text{cm}^{-2} \geq 16.3$  for  $b = 25$  km s $^{-1}$ . Our criteria therefore encompass the fact that the absorbers we located may be sub-LLS, making our limits conservative. In the future, we will employ numerical simulations to forward-model our individual free path procedure; the requirement for accurately predicting  $b$  across a large range of densities necessitates novel radiation-tracing hydro-dynamical simulations which are beyond the scope of this work.

*Uncertainties in model parameters:* We assume fixed values of  $\alpha_{\text{UV}} = 0.6$  and  $\alpha_{\text{ion}} = 1.5$  corresponding to the composite spectrum of Lusso et al. (2015). Both of these values are consistent with constraints from the wider literature (e.g.  $\alpha_{\text{UV}}$ : Vanden Berk et al. 2001; Shull et al. 2012;  $\alpha_{\text{ion}}$ : Telfer et al. 2002). The spread between different composite studies are  $\Delta\alpha_{\text{UV}} \simeq 0.3$  and  $\Delta\alpha_{\text{ion}} \simeq 0.5$ . A systematic shift of both power-law indices to their +1 $\sigma$  range would effectively result in an offset in our computed  $M_{1450}$  of  $\sim 0.3$ , insufficient to alter our results significantly. Differences in continuum properties among quasars will (effectively) lead to scatter in  $M_{1450}$  which may alter the membership of individ-

ual sightlines to bins of emissivity; however, none of the quasars near the edges of the magnitude bins are exceptional compared to the neighbouring bin (see Fig. 2). Confounding factors due to scatter in quasar emission properties can be alleviated by using larger samples in future work.

The uncertainty in  $\Gamma_{\text{bg}}$  is potentially large. We use the value  $\Gamma_{\text{bg}} = 3 \times 10^{-13} \text{ s}^{-1}$  which was most recently computed by Becker et al. (2021) using the Sherwood simulation (Bolton et al. 2017). This value of  $\Gamma_{\text{bg}}$  is calibrated to match the mean Ly- $\alpha$  optical depth measured by Bosman et al. (2018) under the assumption of a spatially homogeneous UVB, and has an uncertainty of  $\sim 40\%$ . However, the Sherwood simulation does not reproduce the observed spatial scatter of Ly- $\alpha$  opacity at  $z = 6$  (Bosman et al. 2021b), suggesting that  $\Gamma_{\text{bg}}$  may be biased. The late reionisation models presented in Kulkarni et al. (2019) and Keating et al. (2020b) successfully match the optical depth scatter, and predict  $\Gamma_{\text{bg}} \simeq 2 \times 10^{-13} \text{ s}^{-1}$ ,  $\Gamma_{\text{bg}} \simeq 3 \times 10^{-13} \text{ s}^{-1}$  respectively (without quantified uncertainties). A change in  $\Gamma_{\text{bg}}$  would directly propagate to our measurements as  $\lambda_{\text{mfp}} \propto \Gamma_{\text{bg}}^{\xi}$ . Our analysis will therefore require revision in the event of significant updates to constraints on  $\Gamma_{\text{bg}}$  at  $z = 6$ .

*Limitations of the formalism:* It is possible for the gas opacity around different quasars to follow different values of  $\xi$ . Dense gas inside proximity zones which was recently ionised by the quasar remains in a significantly non-relaxed state for  $\gtrsim 10^4$  years after quasar turn-on. Significant non-relaxation may lead to a lower effective value of  $\xi$  compared to quasars which have been on continuously for  $\gtrsim 10^7$  years (D’Aloisio et al. 2020; see also Becker et al. 2021). Indeed, two of the quasars in our sample have been argued to have particularly short current lifetimes  $t < 10^4$  years based on the short extent of their proximity zones (Eilers et al. 2021a). If quasar flickering on such timescales is common, the state of gas within proximity zones may not be well described by a single choice of  $\xi$ . We note, however, that (1) the two ‘young’ quasars included in this work provided limits of individual free paths which were indistinguishable from the quasars which are not ‘young’ in our sample; and (2) such an effect would only weaken our lower limits, making our parameters constraints overly conservative. Theoretical explorations of the effect of a flickering quasar phase on the surrounding gas are an active area of research (e.g. Davies et al. 2020; Chen 2020); integrating non-equilibrium effects into a model of the IGM is beyond the scope of this work. We also neglect contributions to the ionisation rate from the galaxy populations which are expected to cluster around high- $z$  quasars.

This contribution is expected to have a moderate impact (Davies 2020), but is non-trivial to model since the dark matter host halo masses of  $z \sim 6$  quasars are not currently known (see e.g. Habouzit et al. 2019).

In addition, we stress that the mean free path computed within the  $\xi$  formalism always refers specifically to the mean free path of ionising photons inside of ionised regions. Spatial fluctuations of  $\Gamma_{\text{bg}}$  in the IGM, such as those induced by ‘islands’ of significantly neutral gas, are not included in the model and cannot impact the resulting constraints on  $\lambda_{\text{mfp}}$ ; in other words,  $\lambda_{\text{mfp}}$  is assumed to not arise from reionisation morphology. Comparisons of constraints obtained within the framework with models in which morphological effects drive  $\lambda_{\text{mfp}}$  is therefore non-trivial.

## 6. CONCLUSIONS

We have introduced a new method for constraining the mean free path of ionising photons at  $z = 6$  using lower limits on the individual free paths. We use the fact that Lyman-limit absorbers with a density sufficient to halt the propagation of ionising photons necessarily produce strong absorption in the 6 lowest-energy Lyman transitions. In the absence of such features, the presence of a Lyman-limit system can be ruled out and a lower limit on the individual free path calculated.

We find that  $\sim 60\%$  of our sample of 26 quasars require individual free paths  $\lambda > 2$  pMpc. In quasars with magnitudes brighter than  $M_{1450} = -26.5$ , the fraction rises to 83% (15/18). Dividing our sample into three magnitude bins containing equal numbers of objects, we use the resulting lower limits on the mean free path around quasars to jointly constrain the mean free path in the background IGM and the scaling of the mean free path on opacity,  $\xi$ . We find constraints on  $\lambda_{\text{mfp}}$  which are in agreement with the measurements of a short  $\lambda_{\text{mfp}}$  by Becker et al. (2021), but our method poses more stringent lower limits on  $\lambda_{\text{mfp}}$ . For the traditionally-assumed value of  $\xi = 2/3$ , we constrain  $\lambda_{\text{mfp}} > 0.31$  (0.18) pMpc at  $2\sigma$  ( $3\sigma$ ). Lower values of  $\xi$  tighten the constraints: for  $\xi = 0.33$  as expected from ionisation non-equilibrium around quasars (D’Aloisio et al. 2020), we constrain  $\lambda_{\text{mfp}} > 1.00$  (0.68) pMpc at  $2\sigma$  ( $3\sigma$ ).

Our limits on  $\lambda_{\text{mfp}}$  are complementary with the approach of stacking transmission at the Lyman limit, as they require no transmission of Lyman continuum to be detected. Individual free path limits can be measured even in the case of overlap with strong Ly- $\alpha$  foreground absorption, as long as quasar possess proximity zones. Independent constraints on  $\lambda_{\text{mfp}}$  and  $\xi$  will be crucial to understanding the IGM at the end stages of reionisation.

1 The author thanks George Becker for sharing his reductions of some of the quasar spectra used in this work and  
 2 for constructive comments on the manuscript. The author is grateful for productive discussions and insightful  
 3 feedback from Frederick Davies, Joe Hennawi and Gábor  
 4 Worseck.  
 5

6 SEIB acknowledges funding from the European Research Council (ERC) under the European Union’s Horizon 2020 research and innovation programme (grant agreement No. 740246 “Cosmic Gas”).  
 7  
 8  
 9  
 10

## APPENDIX

### A. FIRST POSSIBLE LOCATIONS OF A LYMAN-LIMIT SYSTEM

Figure 4 the location of the first LLS absorptions in Ly- $\alpha$  through Ly- $\zeta$ , based on non-detection criteria over three pixels in each transition as explained in the main text. For 7 quasars where the presence of significant Lyman continuum transmission spikes helped to refine the constraints, we indicate the location of the transmission spike redshift with orange vertical bars.

### B. LYMAN CONTINUUM TRANSMISSION SPIKES

Figure 5 shows the Lyman-continuum transmission detected in 7 quasars as listed in Table 1. The criteria for detection are features detected in 6 consecutive pixels at  $1\sigma$ , and a significance of  $4\sigma$  for the emission feature overall.

## REFERENCES

- Alvarez, M. A., & Abel, T. 2012, *ApJ*, 747, 126, doi: [10.1088/0004-637X/747/2/126](https://doi.org/10.1088/0004-637X/747/2/126)
- Bañados, E., Venemans, B. P., Morganson, E., et al. 2015, *ApJ*, 804, 118, doi: [10.1088/0004-637X/804/2/118](https://doi.org/10.1088/0004-637X/804/2/118)
- Bañados, E., Venemans, B. P., Decarli, R., et al. 2016, *ApJS*, 227, 11, doi: [10.3847/0067-0049/227/1/11](https://doi.org/10.3847/0067-0049/227/1/11)
- Becker, G. D., Bolton, J. S., Madau, P., et al. 2015, *MNRAS*, 447, 3402, doi: [10.1093/mnras/stu2646](https://doi.org/10.1093/mnras/stu2646)
- Becker, G. D., D’Aloisio, A., Christenson, H. M., et al. 2021, arXiv e-prints, arXiv:2103.16610. <https://arxiv.org/abs/2103.16610>
- Becker, G. D., Davies, F. B., Furlanetto, S. R., et al. 2018, *ApJ*, 863, 92, doi: [10.3847/1538-4357/aacc73](https://doi.org/10.3847/1538-4357/aacc73)
- Becker, G. D., Pettini, M., Rafelski, M., et al. 2019, *ApJ*, 883, 163, doi: [10.3847/1538-4357/ab3eb5](https://doi.org/10.3847/1538-4357/ab3eb5)
- Boera, E., Becker, G. D., Bolton, J. S., & Nasir, F. 2019, *ApJ*, 872, 101, doi: [10.3847/1538-4357/aafef4](https://doi.org/10.3847/1538-4357/aafef4)
- Bolton, J. S., Becker, G. D., Raskutti, S., et al. 2012, *MNRAS*, 419, 2880, doi: [10.1111/j.1365-2966.2011.19929.x](https://doi.org/10.1111/j.1365-2966.2011.19929.x)
- Bolton, J. S., Becker, G. D., Wyithe, J. S. B., Haehnelt, M. G., & Sargent, W. L. W. 2010, *MNRAS*, 406, 612, doi: [10.1111/j.1365-2966.2010.16701.x](https://doi.org/10.1111/j.1365-2966.2010.16701.x)
- Bolton, J. S., Puchwein, E., Sijacki, D., et al. 2017, *MNRAS*, 464, 897, doi: [10.1093/mnras/stw2397](https://doi.org/10.1093/mnras/stw2397)
- Bosman, S. E. I., Becker, G. D., Haehnelt, M. G., et al. 2017, *MNRAS*, 470, 1919, doi: [10.1093/mnras/stx1305](https://doi.org/10.1093/mnras/stx1305)
- Bosman, S. E. I., Fan, X., Jiang, L., et al. 2018, *MNRAS*, 479, 1055, doi: [10.1093/mnras/sty1344](https://doi.org/10.1093/mnras/sty1344)
- Bosman, S. E. I., Ďurovčíková, D., Davies, F. B., & Eilers, A.-C. 2021a, *MNRAS*, 503, 2077, doi: [10.1093/mnras/stab572](https://doi.org/10.1093/mnras/stab572)
- Bosman, S. E. I., Davies, F. B., Becker, G. D., et al. 2021b, arXiv e-prints, arXiv:2108.03699. <https://arxiv.org/abs/2108.03699>
- Cain, C., D’Aloisio, A., Gangolli, N., & Becker, G. D. 2021, arXiv e-prints, arXiv:2105.10511. <https://arxiv.org/abs/2105.10511>
- Calverley, A. P., Becker, G. D., Haehnelt, M. G., & Bolton, J. S. 2011, *MNRAS*, 412, 2543, doi: [10.1111/j.1365-2966.2010.18072.x](https://doi.org/10.1111/j.1365-2966.2010.18072.x)
- Carnall, A. C., Shanks, T., Chehade, B., et al. 2015, *MNRAS*, 451, L16, doi: [10.1093/mnrasl/slv057](https://doi.org/10.1093/mnrasl/slv057)
- Chen, H. 2020, *ApJ*, 893, 165, doi: [10.3847/1538-4357/ab80c6](https://doi.org/10.3847/1538-4357/ab80c6)



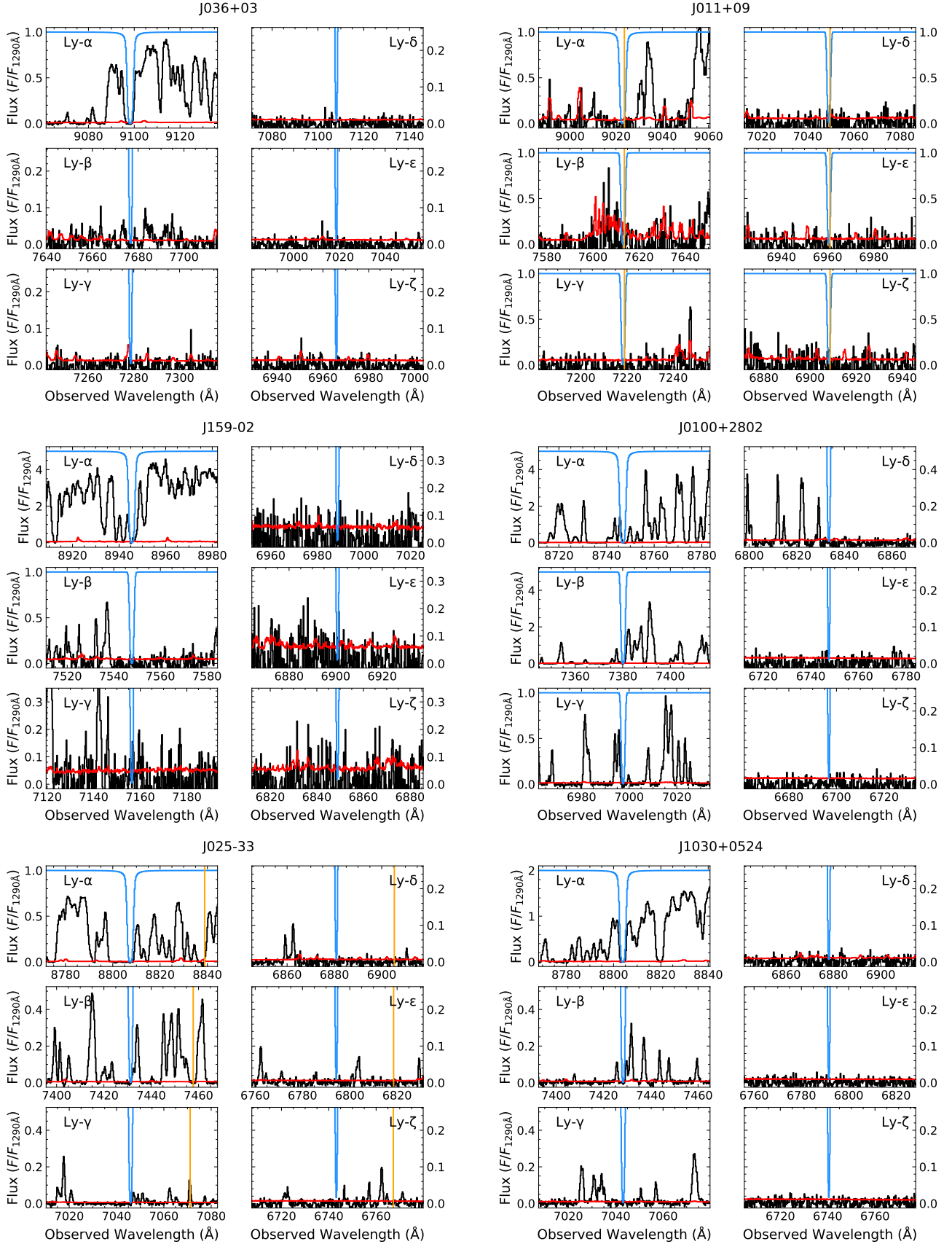
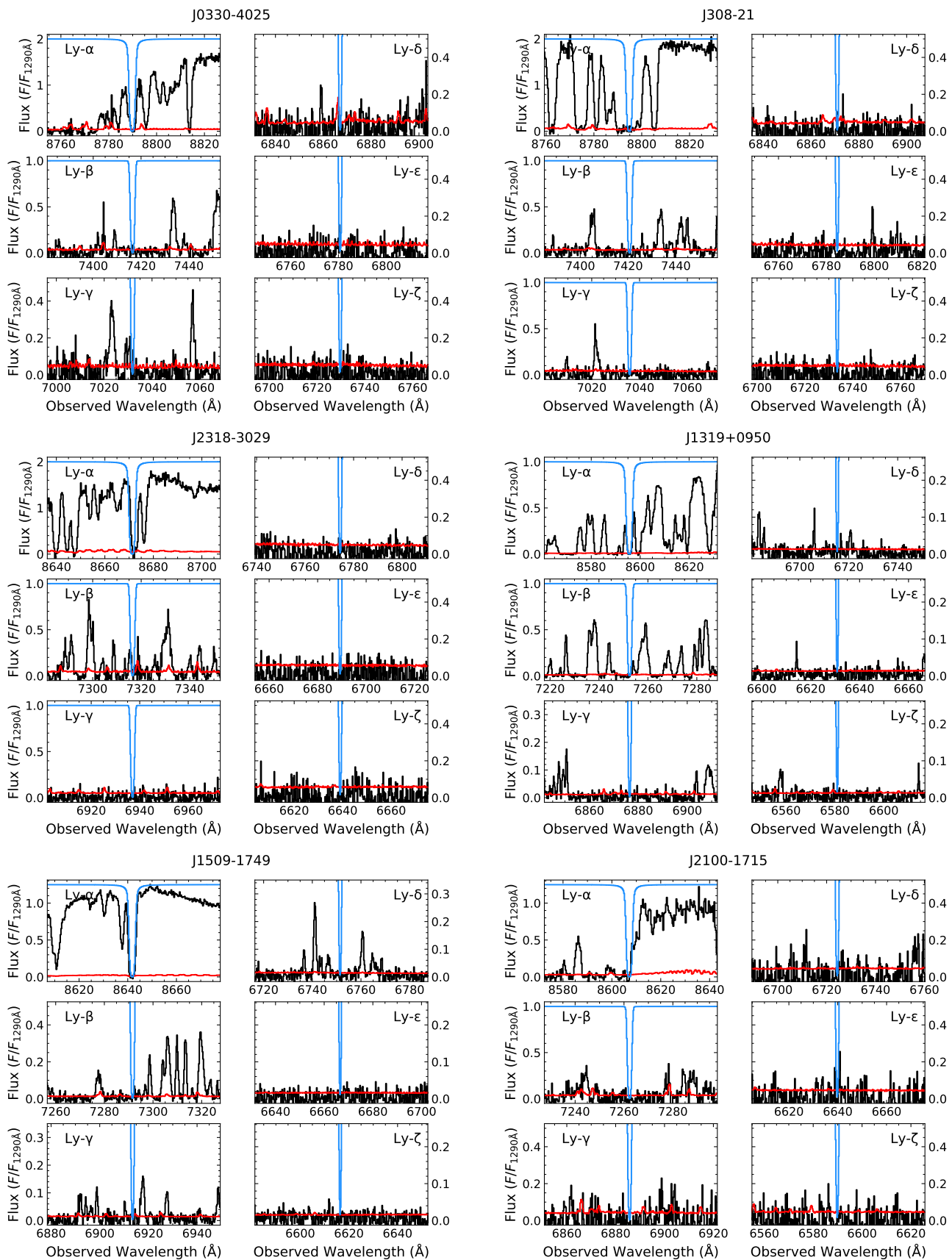


Figure 4. Same as Figure 1 for all quasars in the sample, in order of decreasing redshift.

Figure 4. *continued*

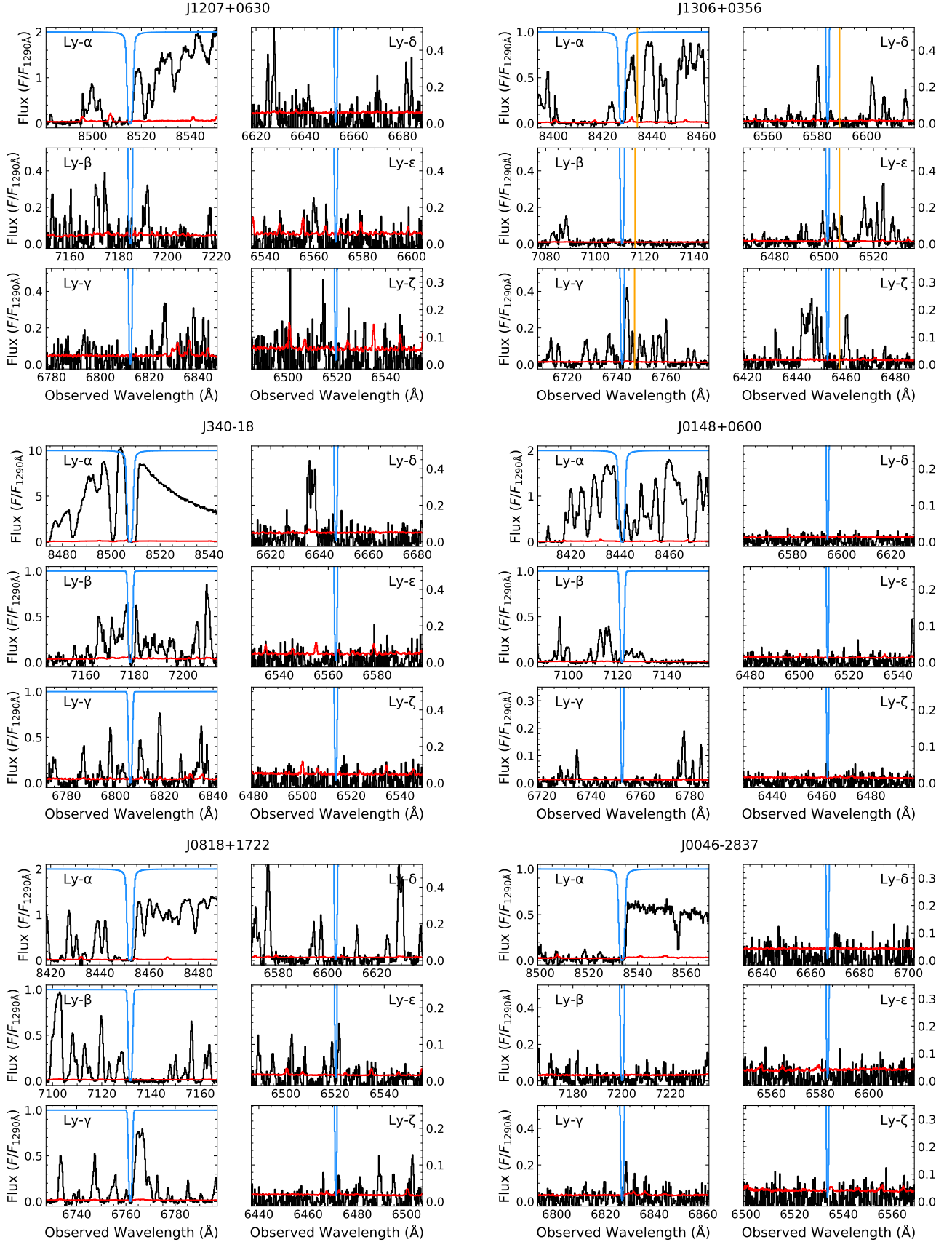


Figure 4. continued

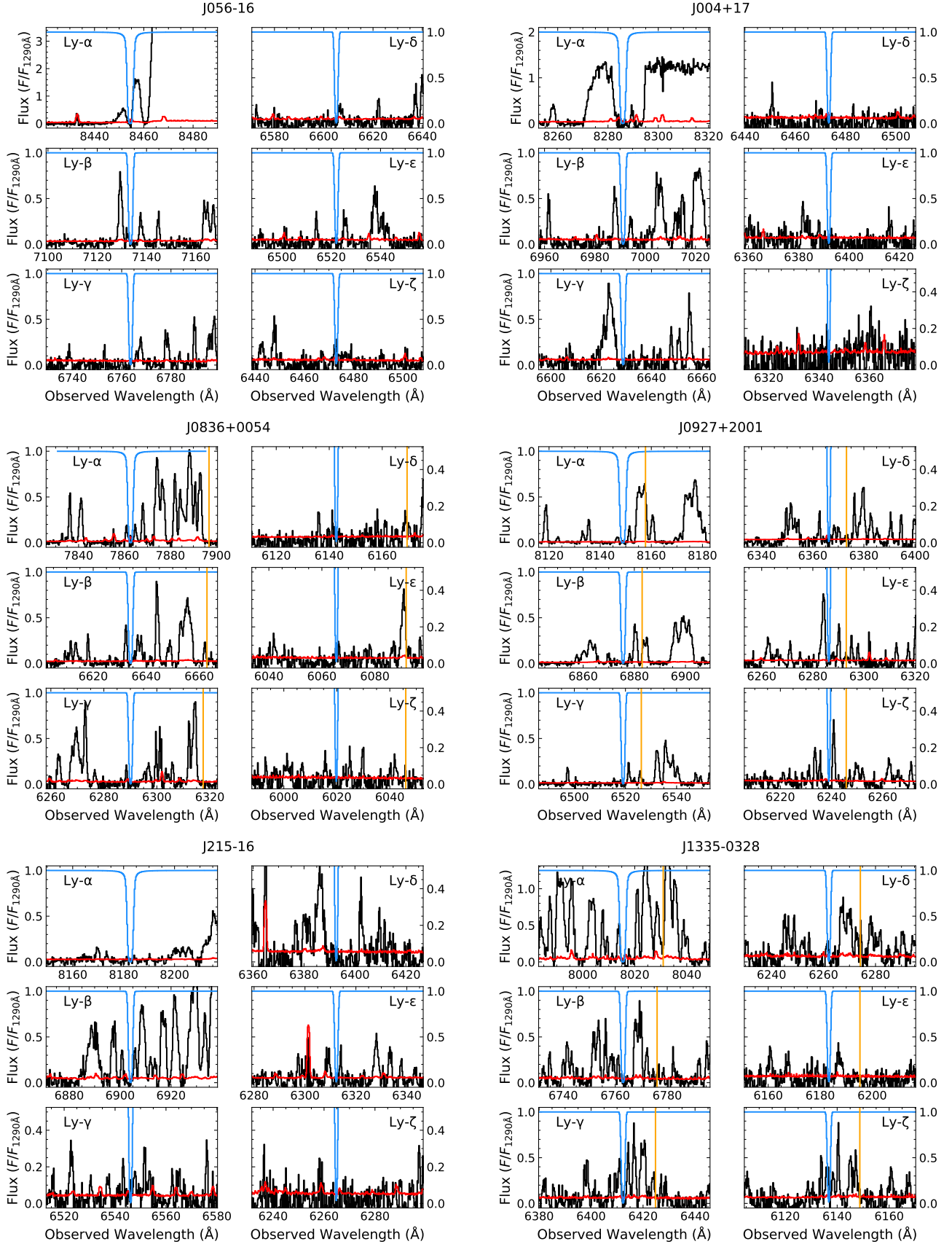


Figure 4. continued



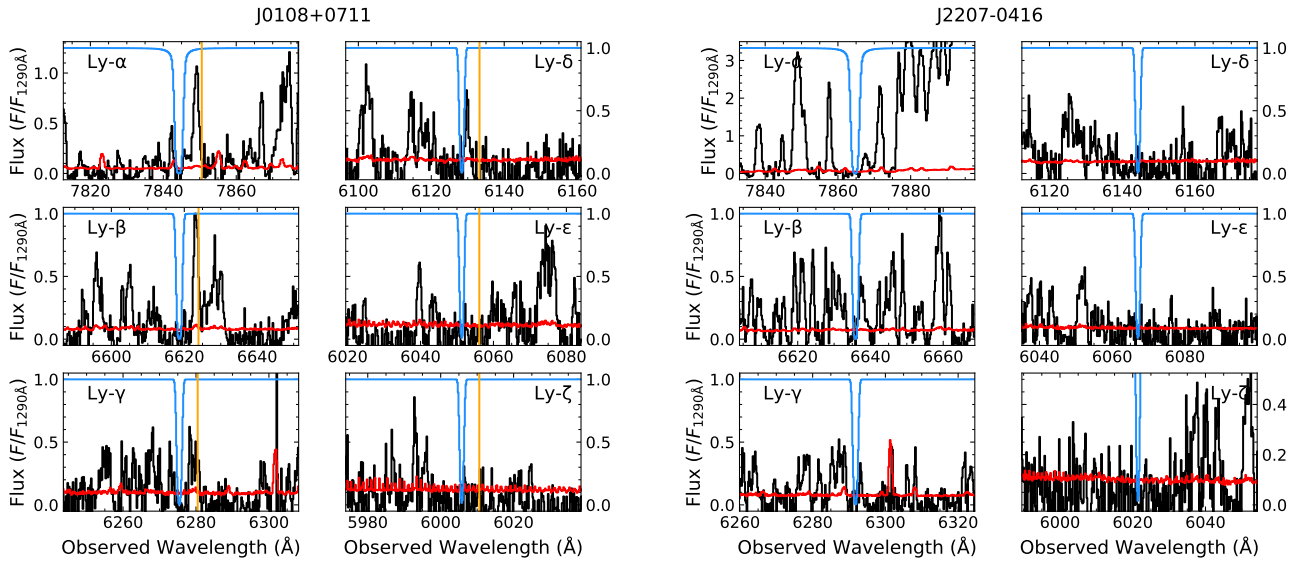
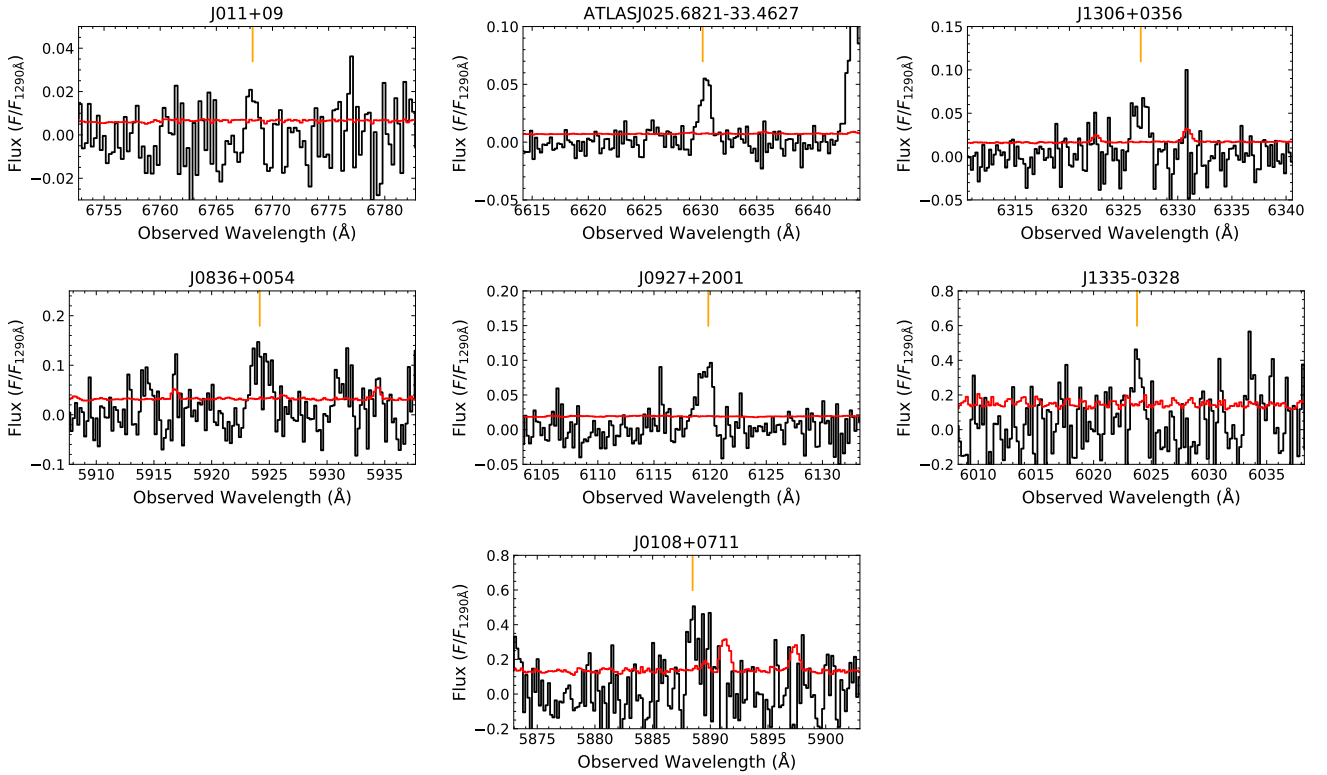
Figure 4. *continued*

Figure 5. Locations of the Lyman-continuum transmission spikes in the 7 quasars for which such features helps strengthen the lower limits on LLS distance (see text).

- D'Aloisio, A., McQuinn, M., Davies, F. B., & Furlanetto, S. R. 2018, *MNRAS*, 473, 560, doi: [10.1093/mnras/stx2341](https://doi.org/10.1093/mnras/stx2341)
- D'Aloisio, A., McQuinn, M., Trac, H., Cain, C., & Mesinger, A. 2020, *ApJ*, 898, 149, doi: [10.3847/1538-4357/ab9f2f](https://doi.org/10.3847/1538-4357/ab9f2f)
- Davies, F. B. 2020, *MNRAS*, 494, 2937, doi: [10.1093/mnras/staa528](https://doi.org/10.1093/mnras/staa528)
- Davies, F. B., Bosman, S. E. I., Furlanetto, S. R., Becker, G. D., & D'Aloisio, A. 2021, arXiv e-prints, arXiv:2105.10518. <https://arxiv.org/abs/2105.10518>
- Davies, F. B., & Furlanetto, S. R. 2014, *MNRAS*, 437, 1141, doi: [10.1093/mnras/stt1911](https://doi.org/10.1093/mnras/stt1911)
- . 2016, *MNRAS*, 460, 1328, doi: [10.1093/mnras/stw931](https://doi.org/10.1093/mnras/stw931)
- Davies, F. B., Hennawi, J. F., & Eilers, A.-C. 2020, *MNRAS*, 493, 1330, doi: [10.1093/mnras/stz3303](https://doi.org/10.1093/mnras/stz3303)
- Decarli, R., Walter, F., Venemans, B. P., et al. 2018, *ApJ*, 854, 97, doi: [10.3847/1538-4357/aaa5aa](https://doi.org/10.3847/1538-4357/aaa5aa)
- Eilers, A.-C., Hennawi, J. F., Davies, F. B., & Simcoe, R. A. 2021a, arXiv e-prints, arXiv:2106.04586. <https://arxiv.org/abs/2106.04586>
- Eilers, A.-C., Hennawi, J. F., Decarli, R., et al. 2020, *ApJ*, 900, 37, doi: [10.3847/1538-4357/aba52e](https://doi.org/10.3847/1538-4357/aba52e)
- . 2021b, *ApJ*, 914, 74, doi: [10.3847/1538-4357/ac05c3](https://doi.org/10.3847/1538-4357/ac05c3)
- Emberson, J. D., Thomas, R. M., & Alvarez, M. A. 2013, *ApJ*, 763, 146, doi: [10.1088/0004-637X/763/2/146](https://doi.org/10.1088/0004-637X/763/2/146)
- Fan, X., Narayanan, V. K., Lupton, R. H., et al. 2001, *AJ*, 122, 2833, doi: [10.1086/324111](https://doi.org/10.1086/324111)
- Fan, X., Strauss, M. A., Becker, R. H., et al. 2006, *AJ*, 132, 117, doi: [10.1086/504836](https://doi.org/10.1086/504836)
- Farina, E. P., Arrigoni-Battaia, F., Costa, T., et al. 2019, *ApJ*, 887, 196, doi: [10.3847/1538-4357/ab5847](https://doi.org/10.3847/1538-4357/ab5847)
- Faucher-Giguère, C.-A., Prochaska, J. X., Lidz, A., Hernquist, L., & Zaldarriaga, M. 2008, *ApJ*, 681, 831, doi: [10.1086/588648](https://doi.org/10.1086/588648)
- Fumagalli, M., O'Meara, J. M., Prochaska, J. X., & Worseck, G. 2013, *ApJ*, 775, 78, doi: [10.1088/0004-637X/775/1/78](https://doi.org/10.1088/0004-637X/775/1/78)
- Furlanetto, S. R., & Oh, S. P. 2005, *MNRAS*, 363, 1031, doi: [10.1111/j.1365-2966.2005.09505.x](https://doi.org/10.1111/j.1365-2966.2005.09505.x)
- Gaikwad, P., Rauch, M., Haehnelt, M. G., et al. 2020, *MNRAS*, 494, 5091, doi: [10.1093/mnras/staa907](https://doi.org/10.1093/mnras/staa907)
- Gnedin, N. Y. 2000, *ApJ*, 535, 530, doi: [10.1086/308876](https://doi.org/10.1086/308876)
- Gnedin, N. Y., & Fan, X. 2006, *ApJ*, 648, 1, doi: [10.1086/505790](https://doi.org/10.1086/505790)
- Haardt, F., & Madau, P. 1996, *ApJ*, 461, 20, doi: [10.1086/177035](https://doi.org/10.1086/177035)
- . 2012, *ApJ*, 746, 125, doi: [10.1088/0004-637X/746/2/125](https://doi.org/10.1088/0004-637X/746/2/125)
- Habouzit, M., Volonteri, M., Somerville, R. S., et al. 2019, *MNRAS*, 489, 1206, doi: [10.1093/mnras/stz2105](https://doi.org/10.1093/mnras/stz2105)
- Jiang, L., Fan, X., Vestergaard, M., et al. 2007, *AJ*, 134, 1150, doi: [10.1086/520811](https://doi.org/10.1086/520811)
- Jiang, L., McGreer, I. D., Fan, X., et al. 2015, *AJ*, 149, 188, doi: [10.1088/0004-6256/149/6/188](https://doi.org/10.1088/0004-6256/149/6/188)
- Jung, I., Finkelstein, S. L., Dickinson, M., et al. 2020, *ApJ*, 904, 144, doi: [10.3847/1538-4357/abbd44](https://doi.org/10.3847/1538-4357/abbd44)
- Kashino, D., Lilly, S. J., Shibuya, T., Ouchi, M., & Kashikawa, N. 2020, *ApJ*, 888, 6, doi: [10.3847/1538-4357/ab5a7d](https://doi.org/10.3847/1538-4357/ab5a7d)
- Keating, L. C., Kulkarni, G., Haehnelt, M. G., Chardin, J., & Aubert, D. 2020a, *MNRAS*, 497, 906, doi: [10.1093/mnras/staa1909](https://doi.org/10.1093/mnras/staa1909)
- Keating, L. C., Weinberger, L. H., Kulkarni, G., et al. 2020b, *MNRAS*, 491, 1736, doi: [10.1093/mnras/stz3083](https://doi.org/10.1093/mnras/stz3083)
- Kulkarni, G., Keating, L. C., Haehnelt, M. G., et al. 2019, *MNRAS*, 485, L24, doi: [10.1093/mnrasl/slz025](https://doi.org/10.1093/mnrasl/slz025)
- Lusso, E., Worseck, G., Hennawi, J. F., et al. 2015, *MNRAS*, 449, 4204, doi: [10.1093/mnras/stv516](https://doi.org/10.1093/mnras/stv516)
- Mazzucchelli, C., Bañados, E., Venemans, B. P., et al. 2017, *ApJ*, 849, 91, doi: [10.3847/1538-4357/aa9185](https://doi.org/10.3847/1538-4357/aa9185)
- McQuinn, M., Hernquist, L., Lidz, A., & Zaldarriaga, M. 2011, *MNRAS*, 415, 977, doi: [10.1111/j.1365-2966.2011.18788.x](https://doi.org/10.1111/j.1365-2966.2011.18788.x)
- Meiksin, A., & Madau, P. 1993, *ApJ*, 412, 34, doi: [10.1086/172898](https://doi.org/10.1086/172898)
- Miralda-Escude, J., & Ostriker, J. P. 1990, *ApJ*, 350, 1, doi: [10.1086/168358](https://doi.org/10.1086/168358)
- Morales, A., Mason, C., Bruton, S., et al. 2021, arXiv e-prints, arXiv:2101.01205. <https://arxiv.org/abs/2101.01205>
- Morganson, E., De Rosa, G., Decarli, R., et al. 2012, *AJ*, 143, 142, doi: [10.1088/0004-6256/143/6/142](https://doi.org/10.1088/0004-6256/143/6/142)
- Mortlock, D. J., Patel, M., Warren, S. J., et al. 2009, *A&A*, 505, 97, doi: [10.1051/0004-6361/200811161](https://doi.org/10.1051/0004-6361/200811161)
- Nasir, F., & D'Aloisio, A. 2020, *MNRAS*, 494, 3080, doi: [10.1093/mnras/staa894](https://doi.org/10.1093/mnras/staa894)
- O'Meara, J. M., Prochaska, J. X., Worseck, G., Chen, H.-W., & Madau, P. 2013, *ApJ*, 765, 137, doi: [10.1088/0004-637X/765/2/137](https://doi.org/10.1088/0004-637X/765/2/137)
- Planck Collaboration, Aghanim, N., Akrami, Y., et al. 2020, *A&A*, 641, A6, doi: [10.1051/0004-6361/201833910](https://doi.org/10.1051/0004-6361/201833910)
- Prochaska, J. X., O'Meara, J. M., & Worseck, G. 2010, *ApJ*, 718, 392, doi: [10.1088/0004-637X/718/1/392](https://doi.org/10.1088/0004-637X/718/1/392)
- Prochaska, J. X., Worseck, G., & O'Meara, J. M. 2009, *ApJL*, 705, L113, doi: [10.1088/0004-637X/705/2/L113](https://doi.org/10.1088/0004-637X/705/2/L113)
- Rahmati, A., Pawlik, A. H., Raičević, M., & Schaye, J. 2013, *MNRAS*, 430, 2427, doi: [10.1093/mnras/stt066](https://doi.org/10.1093/mnras/stt066)
- Rahmati, A., & Schaye, J. 2018, *MNRAS*, 478, 5123, doi: [10.1093/mnras/sty1382](https://doi.org/10.1093/mnras/sty1382)

- Reed, S. L., McMahon, R. G., Martini, P., et al. 2017, MNRAS, 468, 4702, doi: [10.1093/mnras/stx728](https://doi.org/10.1093/mnras/stx728)
- Romano, M., Grazian, A., Giallongo, E., et al. 2019, A&A, 632, A45, doi: [10.1051/0004-6361/201935550](https://doi.org/10.1051/0004-6361/201935550)
- Rudie, G. C., Steidel, C. C., Shapley, A. E., & Pettini, M. 2013, ApJ, 769, 146, doi: [10.1088/0004-637X/769/2/146](https://doi.org/10.1088/0004-637X/769/2/146)
- Schindler, J.-T., Farina, E. P., Bañados, E., et al. 2020, ApJ, 905, 51, doi: [10.3847/1538-4357/abc2d7](https://doi.org/10.3847/1538-4357/abc2d7)
- Shull, J. M., Stevans, M., & Danforth, C. W. 2012, ApJ, 752, 162, doi: [10.1088/0004-637X/752/2/162](https://doi.org/10.1088/0004-637X/752/2/162)
- Songaila, A., & Cowie, L. L. 2010, ApJ, 721, 1448, doi: [10.1088/0004-637X/721/2/1448](https://doi.org/10.1088/0004-637X/721/2/1448)
- Telfer, R. C., Zheng, W., Kriss, G. A., & Davidsen, A. F. 2002, ApJ, 565, 773, doi: [10.1086/324689](https://doi.org/10.1086/324689)
- Vanden Berk, D. E., Richards, G. T., Bauer, A., et al. 2001, AJ, 122, 549, doi: [10.1086/321167](https://doi.org/10.1086/321167)
- Venemans, B. P., Verdoes Kleijn, G. A., Mwebaze, J., et al. 2015, MNRAS, 453, 2259, doi: [10.1093/mnras/stv1774](https://doi.org/10.1093/mnras/stv1774)
- Venemans, B. P., Decarli, R., Walter, F., et al. 2018, ApJ, 866, 159, doi: [10.3847/1538-4357/aadf35](https://doi.org/10.3847/1538-4357/aadf35)
- Venemans, B. P., Walter, F., Neeleman, M., et al. 2020, ApJ, 904, 130, doi: [10.3847/1538-4357/abc563](https://doi.org/10.3847/1538-4357/abc563)
- Vernet, J., Dekker, H., D’Odorico, S., et al. 2011, A&A, 536, A105, doi: [10.1051/0004-6361/201117752](https://doi.org/10.1051/0004-6361/201117752)
- Wang, F., Wu, X.-B., Fan, X., et al. 2016, ApJ, 819, 24, doi: [10.3847/0004-637X/819/1/24](https://doi.org/10.3847/0004-637X/819/1/24)
- Willott, C. J., Delorme, P., Omont, A., et al. 2007, AJ, 134, 2435, doi: [10.1086/522962](https://doi.org/10.1086/522962)
- Willott, C. J., Delorme, P., Reyl  , C., et al. 2010, AJ, 139, 906, doi: [10.1088/0004-6256/139/3/906](https://doi.org/10.1088/0004-6256/139/3/906)
- Worseck, G., Prochaska, J. X., O’Meara, J. M., et al. 2014, MNRAS, 445, 1745, doi: [10.1093/mnras/stu1827](https://doi.org/10.1093/mnras/stu1827)
- Wu, X.-B., Wang, F., Fan, X., et al. 2015, Nature, 518, 512, doi: [10.1038/nature14241](https://doi.org/10.1038/nature14241)
- Yang, J., Fan, X., Wu, X.-B., et al. 2017, AJ, 153, 184, doi: [10.3847/1538-3881/aa6577](https://doi.org/10.3847/1538-3881/aa6577)